Computing and Informatics, Vol. 43, 2024, 1372–1396, doi: 10.31577/cai_2024_6_1372

LOWER LIMB MOTOR INTENTION DETECTION MODEL BASED ON FEATURE FUSION AND REINFORCEMENT LEARNING ASSISTED APPROACH

Liujie Cheng, Hongfei Ji

College of Electronic and Information Engineering, Tongji University
Shanghai 201804, China
e-mail: {2132926, jhf}@tongji.edu.cn

Jie Li

College of Electronic and Information Engineering, Tongji University
Shanghai 201804, China
&
Translational Research Center, Shanghai Yangzhi Rehabilitation Hospital
Shanghai Sunshine Rehabilitation Center
Tongji University, Shanghai, China
e-mail: nijanice@163.com

Jian Yu*

College of Electronic and Information Engineering, Tongji University
Shanghai 201804, China
e-mail: yujian@tongji.edu.cn

Zilong Pang

School of Software, Intelligent Data Processing Engineering Research Center of Henan Province, Henan University, Kaifeng, 475004, China
e-mail: jszxpzl@henu.edu.cn

Abstract. Brain-computer interface (BCI) technology holds immense promise in the rehabilitation of patients with movement disorders, leveraging the body's physiological mechanisms to enhance their quality of life by reshaping motor neural circuits through external devices. Nevertheless, current BCI applications for rehabilitation predominantly rely on a single physiological signal, often overlooking the synergistic impact of multiple signals. Simultaneously, while reinforcement learning shows significant potential for BCI applications, there exists a scarcity of studies exploring this intersection.This paper introduces a novel motor intention judgment model grounded in multimodal signal fusion and reinforcement feature selection. The model adeptly extracts comprehensive motor intention features by integrating pertinent information from both electroencephalogram (EEG) and electromyogram (EMG). Furthermore, reinforcement learning is employed for judicious feature selection, yielding promising outcomes in subsequent experiments. The study utilizes publicly available datasets to diagnose the motion intention of the subjects, complemented by ablation experiments to affirm the efficacy of the model components. In instances of feature-level fusion, the model demonstrated a noteworthy enhancement in the average five-classification accuracy, surpassing results obtained from isolated EEG and EMG experiments by 28.46 % and 12.68 %, respectively. The primary objective of this research is to furnish robust model support for motor rehabilitation training with exoskeletons, offering personalized solutions for the restoration of motor functions.

Keywords: Hybrid BCI, EEG, EMG, reinforcement learning, feature fusion, feature selection

Mathematics Subject Classification 2010: 68-T10

1 INTRODUCTION

The Brain-Computer Interface (BCI) is an advanced technology employing specialized equipment to facilitate information interaction between the nervous system and external devices, establishing a direct link between the brain and external devices without traversing the brain's typical peripheral neural and muscular output pathways [1]. This technology captures brain neural activity signals through sensors and employs advanced machine learning and pattern recognition algorithms to discern these signals during different cognitive activities. Subsequently, it translates them into control commands, facilitating direct communication between the human brain and external devices. Currently, BCI technology holds significant research value in diverse fields such as emotion recognition [2], sleep state recognition [3], smart cities [4], disease diagnosis [5], and healthcare [6]. Notably, BCI technology exhibits considerable potential in motor rehabilitation [7, 8], providing a novel communication channel and rehabilitation method for individuals facing physical challenges.

* Corresponding author

Among the various BCI types, hybrid BCI stands out as a popular choice. This type enhances the accuracy of individual state judgment by amalgamating BCIs capable of capturing different physiological signals, adapting them to more complex usage scenarios and thereby enhancing the practical usability of BCIs [9]. Hybrid BCIs manifest in various forms, and this paper specifically delves into the combination of EEG-based BCIs and EMG-based BCIs, which represents one of the more common and impactful combinations [10].

Hybrid BCI introduces a groundbreaking concept in utilizing brain-computer interface technology for exercise rehabilitation, a notion that has garnered significant attention from researchers [10, 11]. Studies have indicated homology between EEG and EMG signals, with EEG demonstrating an earlier response time than EMG signals in limb movement intention [12]. Furthermore, intriguingly, even in cases where a patient has lost a limb, the brain continues in sending signals to the absent limb [13]. These research findings collectively provide a theoretical foundation for the viability of BCI-assisted motor rehabilitation. Currently, researchers have delved into the integration of BCIs with exoskeletons, declaring that BCIs hold unique applications and practical value within the system as a communication and control method for individuals with physical disabilities [14]. A crucial component of converting physiological signals into control signals for rehabilitation equipment involves the implementation of a motion intent detection algorithm. This algorithm plays a pivotal role in seamlessly translating physiological signals into control signals, facilitating the effective operation of rehabilitation equipment.

In the realm of motion intent detection algorithms, two predominant approaches have emerged: traditional machine learning methods and deep learning methods. The former relies on manual signal processing and feature extraction, necessitating researchers to undertake tasks such as artifact removal, re-referencing, and bandpass filtering on the acquired signals [15]. Several traditional methods are employed for extracting features from physiological signals, including Common Spatial Pattern (CSP) [16], Short-Time Fourier Transform [17], Principal Component Analysis [18], and supervised classification using traditional machine learning methods [19]. Conversely, the latter approach, based on deep learning methods, streamlines the process with fewer mandatory steps. Preprocessing of acquired signals becomes optional and can be tailored to the specific objectives of the experiment. Feature extraction, in this context, entirely relies on the functionality of the neural network employed in the system. This dichotomy reflects the evolving landscape in motion intent detection algorithms, offering researchers flexibility in choosing methodologies that align with their experimental goals and resource constraints.

Presently, significant strides have been made in the realm of physiological signal classification, primarily driven by advancements in deep learning and related algorithms. A myriad of neural network architectures, including Convolutional Neural Networks (CNN) [20] and Recurrent Neural Networks (RNN) [21], have been successfully applied to the classification of physiological signals. Lawhern et al. [22] introduced EEG-NET, a model for EEG classification, leveraging multiple convolutional layers, and validated its performance across diverse paradigm datasets.

Chen et al. [23] utilized a recurrent convolutional neural network to extract spatio-temporal features from physiological signals, demonstrating its efficacy in identifying subjects' emotions. Sairamya et al. [24] constructed an artificial neural network analyzing physiological signal features extracted by discrete wavelet transform, offering an auxiliary method for diagnosing schizophrenia. Neeraj et al. [25] advanced the field by incorporating the Attention mechanism into the network, presenting the CNN-LSTM-ATT network for judging physiological signals of alcoholics. However, the inherent limitations of physiological signals, such as the non-smoothness of EEG signals, signal uniqueness, and the relatively small size of physiological signal datasets, necessitate the implementation of methods to better extract information from these signals [26]. For instance, transfer learning [27] methods enhance classifier learning performance by projecting samples from source and target domains into a common domain, addressing the challenge posed by small dataset sizes. Beyond transfer learning, researchers have explored the utility of small samples [28], semi-supervised [29], and unsupervised [30] methods in conjunction with BCI to address the aforementioned challenges. These approaches collectively contribute to overcoming the intricacies associated with physiological signals, thereby advancing the capabilities of motion intent detection algorithms.

Among various deep learning methods, reinforcement learning stands out as a particularly promising approach [31]. Its iterative nature allows the reinforcement learning framework to identify task-relevant segments from given physiological signals and provide appropriately defined reward signals [32]. Notably, some studies have leveraged reinforcement learning to enhance the judgment and recognition of physiological signals. For instance, Wang et al. [33] proposed a neural network search algorithm based on the Q-learning algorithm to assist in constructing a neural network for recognizing surface electromyography (sEMG) signals. While their study did not delve into the physiological signals themselves, it focused on optimizing the parameters of the neural network for improvement. Zhang et al. [34] employed a model-free reinforcement learning approach to implement a control algorithm for hip exoskeletons, yet the main contributors remained the kinematic parameters, not fully reflecting the potential value of BCI, despite the use of EMGs for assisted training. Ming et al. [35] used a Q-learning algorithm to assess subjects' attention, concentrating on attention-related EEGs without expanding into motor-related signals. Similarly, Ko et al.'s [36] feature selection of motor imagery signals using the actor-critic model was groundbreaking, but their focus was limited to EEG and motor imagery signals, overlooking EMG and motor execution signals. Addressing the shortcomings of the aforementioned literature, this paper introduces a motion intention judgment model grounded in multimodal signal fusion and reinforcement feature selection. By concurrently harnessing information from EEG and EMG, complemented by reinforcement learning to select signal fragments with pertinent information, the proposed model facilitates motion intention detection. Experimental validations conducted on publicly available datasets attest to the model's robust performance, thereby offering a comprehensive and effective solution in the domain of motion intention judgment.

The subsequent sections of this paper are structured as follows. The second section introduces the methodology adopted in this study. It encompasses the theory of physiological signal fusion, an overview of the comprehensive model architecture, and a detailed exposition of each component comprising the model. The third section elucidates the datasets employed for experimental validation. It delves into a comprehensive discussion and analysis of the experimental results, providing insights into the model's performance. The fourth section encapsulates the conclusions drawn from the study. Additionally, it outlines future directions for research, offering a perspective on potential advancements in the field. This organizational structure is designed to provide readers with a systematic and coherent understanding of the research methodology, results, and implications presented in this paper.

2 METHOD

In this section, we propose a classification model based on multimodal signals with reinforcement learning. The model leverages reinforcement learning for feature selection and employs a feature fusion method to enhance the classification performance on multimodal data. The entire model is structured into three distinct modules: the feature extraction module, the feature selection module, and the classifier module. The subsequent sections provide an in-depth exploration of the overall model framework. Let us consider a trial of data denoted as $X \in R^{C \times T}$, where C represents the number of leads, and T is the number of sampling points. Upon inputting X into the network, it initially enters the feature extraction module, concurrently undergoing a feature fusion operation to yield the feature vector V. Subsequently, the extracted feature vector V is directed to the feature selection module, where the reinforcement learning method is applied to extract the most pertinent vector V' for the target task. Finally, the resulting feature vector V' is forwarded to the classifier module to execute the classification process. This modular architecture facilitates a streamlined and effective approach to handling multimodal signals, optimizing feature selection through reinforcement learning, and ultimately improving the overall classification performance.

2.1 The Theory of Feature Fusion

Drawing upon the theories presented in several articles [37, 38], we distill various approaches to feature fusion into three categories: data-level, feature-level, and decision-level. To illustrate these approaches, we employ a simple Convolutional Neural Network (CNN) as an example. The network comprises a CNN layer for feature extraction and a fully connected layer with Softmax for learning and classification.In the data-level fusion method, input data is fused before being processed by the network. The fused data undergoes feature extraction, and the extracted features are utilized for classification; for the feature-level fusion method, each type of data possesses an independent feature extractor, potentially leveraging different

algorithms for feature extraction. Features from each data type are extracted independently and then fused, and the fused features are employed for classification; in the decision-level method, each type of data is associated with its exclusive deep learning structure, akin to integrated learning. Decision-level fusion involves combining the output of each network, culminating in the final result. Figure 1 shows the structure of the three approaches described above. This classification and illustration provide a comprehensive overview of the three fundamental strategies for feature fusion in the context of neural network architectures.

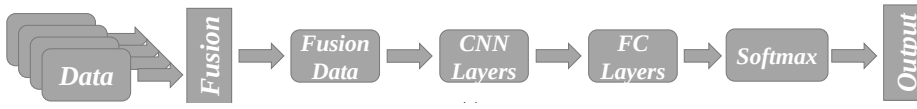

a) Data-level fusion method

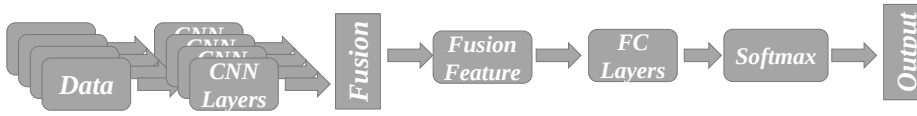

b) Feature-level fusion method

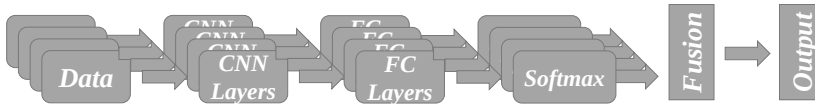

c) Decision-level fusion method

Figure 1. Flowcharts of fusion methods

Next, we delve into the fusion of EEG and EMG, elucidating the distinctions between various feature fusion approaches. Considering data-level fusion, let $X_{eeg} \in R^{C_{eeg} \times T}$ represent EEG data and $X_{emg} \in R^{C_{emg} \times T}$ denote EMG data. The fused data is represented as $X_{fusion} = (X_{eeg}, X_{emg}), X_{fusion} \in R^{(C_{eeg}+C_{emg}) \times T}$, which can be considered as adopting the splicing approach.

For feature-level fusion, let the extracted EEG features be denoted as $V_{eeg} = \{v_1, v_2, \ldots, v_n\}$, with n being the number of feature components. Similarly, the EMG features are represented as $V_{emg} = \{v'_1, v'_2, \ldots, v'_n\}$. Employing feature summation, we obtain $V_{fusion} = V_{eeg} + V_{emg} = \{v_1 + v'_1, v_2 + v'_2, \ldots, v_n + v'_n\}$. This approach enhances information within the feature vectors. If a specific component feature is not salient, the feature selection module can recognize it faster with doubled component information.

For decision-level fusion, let $y_{eeg} = argmax(P_{eeg}) = argmax(\{p_1, p_2, \ldots, p_m\})$ represent the prediction result of the EEG branch, where m is the number of categories. Similarly, $y_{emg} = argmax(P_{emg}) = argmax(\{p'_1, p'_2, \ldots, p'_m\})$ is the prediction result of the EMG branch. An integrated learning-like approach is employed to synthesize probabilities from both branches, resulting in $y_{fusion} = argmax(P_{eeg} +$

$P_{emg}) = argmax(\{p_1 + p'_1, p_2 + p'_2, \ldots, p_m + p'_m\})$. The most likely category is determined by integrating the largest probability value, yielding the final classification result.

Comparing fusion features (X_{fusion}, V_{fusion}, y_{fusion}) with non-fusion features (X, V, y), fusion features contain more information, both positive and negative. However, in the subsequent feature selection module, positive features are retained, and negative features are discarded whenever possible. This selective retention of positive features is the key factor contributing to the enhanced effectiveness of feature fusion.

2.2 Feature Extraction Module

Our feature extraction module is based on the Multiscale Feature Extraction Network (MSNN) [39], as illustrated in Figure 2. The structure of this network is rooted in the residual theory, designed to derive more comprehensive and hierarchical classification features by concatenating feature vectors with varying extraction depths. The network comprises two main modules: the time-domain feature characterization module and the spatial feature characterization module. The input data initially enters this module, where the temporal correlation characteristics of the data are extracted. Multiple convolutional layers are employed within this module. After the first layer, the output of each subsequent layer flows into the spatial feature characterization module, showcasing the embodiment of the residual idea. Spatial feature characterization module informed by the residual theory, receives the output from each layer of the time-domain feature characterization module. The residual idea is realized in this module, contributing to the generation of more holistic and hierarchically structured classification features.

Given the input data $X \in R^{C \times T}$, in the time-domain feature characterization module, only the time-domain dimension of the input data is targeted, so the dimension of the convolution kernel is set to be $(1 \times T)$, where T_i is the size of the convolution kernel set in the ith convolutional layer. After each round of time-domain convolution, the time-domain information in the data will be more condensed, however, the information in other dimensions of the data will be impaired, and at the same time the spatial dimension features of the physiological electrical signals are equally important, so the spatial feature characterization module is introduced, which utilizes the idea of residuals to extract the information of the data at multiple levels, and at the same time, sets specific convolution kernels to extract the spatial features in the data. For the output $X' \in R^{C \times T'}$ of the previous module, for the spatial characterization information contained in it, a convolution kernel with dimension $(C \times 1)$ is used for the extraction operation. Each convolutional layer in the spatial feature characterization module extracts the spatial information of the corresponding layer of data and places the extracted features into the pending region. After the process of the spatial feature characterization module is completed, all the feature vectors in the pending region are spliced together according to a certain rule, so that we obtain the feature vector V for feature selection to be

performed.

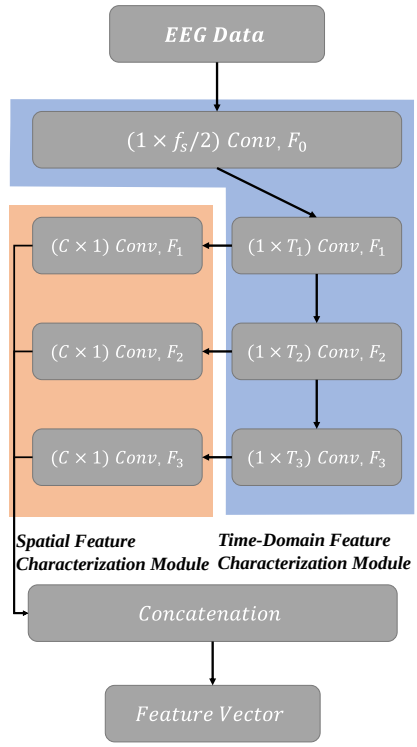

Figure 2. The proposed architectural framework of our feature extraction module

2.3 Feature Selection Module

In the feature selection module, we introduce a reinforcement learning method for selecting task-relevant features, and also inspired by [36], we revamped the feature selection module. For the feature vector $V = \{v_1, v_2, v_3, \ldots, v_{T''}\} \in R^{C'' \times T'' \times D}$, where C'', T'', and D are the number of channels after convolution, the number of sampling points after convolution, and the number of convolutionally spliced number of feature maps, we use a method of feature segmentation according to the time point t, where t belongs to P, $P \subset \{1, 2, 3, \ldots, T''\}$. For physiological signals, not all segments contain valid information, and the differences in physiological conditions between people make the localization of valid features not traceable. Therefore, we utilize the properties of reinforcement learning, which can be used to filter task-relevant features in a label-free environment using a feedback learning decision strategy with a reward function. Briefly, it is the process in which an intelligent body makes action decisions in a series of states, receives feedback from

the reward function after interacting with the environment, and uses the feedback to continuously and iteratively learn, as shown in Figure 3. In the following, we deconstruct the whole learning process into states, actions, reward functions, and learning strategies to illustrate them one by one.

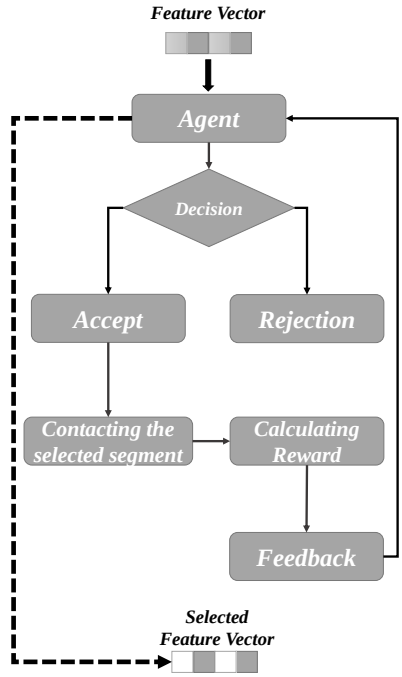

Figure 3. The flowchart of our feature selection module

2.3.1 State

The state S_t in this model, where $t = \{1, 2, 3, \ldots, T''\}$ can be defined as the concatenation of the ensemble of feature vectors selected at the previous time point i.e., $Set\left(\{v_i\}_{i\in P_{t-1}}\right)$ with the new conjunction formed by the above ensemble plus the feature vectors at point t. It can also be denoted as

$$S_t = Cont\left(Set\left(\{v_i\}_{i\in P_{t-1}}\right), Set\left(\{v_i\}_{i\in P_{t-1}} \cup \{v_t\}\right)\right),$$

where $Cont$ is the tandem operation and P_{t-1} is the time point selected in the previous round, as for the Set operation, it can be defined as that

$$Set\left(\{v_i\}_{i\in P_t}\right) = \frac{1}{|P_t|}\sum_{i\in P_t} v_i,$$

where $|P_t|$ is the length of P_t. For the state, stitching together the features with and without the current time point features contains enough information for the intelligence to make a correct decision.

2.3.2 Action

The action space is the set of actions that the agent can make, which we define here as the information about whether the agent accepts the feature corresponding to the current point in time, i.e.

$$a_t = \begin{cases} 0, & \text{rejection}, \\ 1, & \text{accept}. \end{cases}$$

And the goal of the whole structure is to find a continuous sequence of actions, so we need to use the feedback of the action reward function at each time point to make a decision on whether to accept the current feature or not. Therefore, we can define the update strategy of the set P_t

$$P_t = \begin{cases} P_{t-1} \cup \{t\}, & \text{if } a_t = 1, \\ P_{t-1}, & \text{if } a_t = 0. \end{cases}$$

2.3.3 Reward

In order to make appropriate feedback to the action of agent, we first do the *Set* operation on the feature vector that does not perform selection, i.e.

$$V_{Origin} = Set\left(\{v_i\}_{i\in\{1,2,3,\ldots,T''\}}\right),$$

and compute the classification loss L_{Origin} based on V_{Origin}. For the computation of the classification loss, we choose the widely used cross-entropy function. And our goal is to formulate the associated rewards according to the classification loss. Therefore, for the action and the corresponding feature vector $Set\left(\{v_i\}_{i\in P_{t-1}}\right)$ at timepoint t, the reward r_t is defined as

$$r_t = L_{Origin} - L_t,$$

where L_t is the classification loss of the feature vector at timepoint t, which is also calculated by the cross-entropy loss function. Ultimately, the expected reward R_t obtained from an epoch of reinforcement learning is

$$R_t = \sum_{k=0}^{T''} \gamma^k r_{t+k},$$

where γ is the discount factor, which is set to attenuate the cumulative effect of future rewards on the current action selection of the intelligent body. That is, more weight is given to the most recent action by gradually decreasing the value of the future reward.

2.3.4 Strategy of Learning

Among many reinforcement learning methods, we choose the actor-critic network. Briefly, the agent maintains a policy network as an actor and a value estimation function as a critic. For timepoint t, the agent receives the environment s_t, selects the most probable one from the action space according to the policy network, a_t. It then receives a reward r_t and receives the next state s_{t+1} in the environment.

In our work, we utilize a simultaneous and parallel actor-critic network. Specifically, two different deep neural networks are used for strategy estimation and expected return or value estimation, respectively. The output neuron of the strategy network corresponds to the probability of taking a selection or rejection action with respect to the current feature vector under state s_t. Meanwhile, the value estimation network has an output neuron that produces the expected return under the current state s_t.

2.4 Classifier Module

After obtaining the feature vector V' that has been selected by the feature selection module, we input it into the global average pooling layer, which can better emphasize the spatio-temporal information of each feature dimension and its correlation with the neighboring parts from the point of view of BCI. After the pooling operation, the feature vectors are put into a classifier consisting of a fully connected layer as well as a Softmax layer, Softmax is a mathematical function typically used to convert a set of arbitrary real numbers into real numbers representing a probability distribution. It is essentially a normalization function that converts a set of arbitrary real values into probability values between $[0, 1]$, with different probabilities indicating the magnitude of the likelihood that this sample is in the corresponding category, and the higher the probability, the greater the likelihood that the sample belongs to that category, with the probabilities summing up to 1. Assuming that $Z^l \in R^K$ is the output of the previous layer, then the Softmax function can be expressed as:

$$Softmax(Z^l)_i = \frac{\mathrm{e}^{z_i}}{\sum_{j=1}^{K-1} \mathrm{e}^{z_j}},$$

where K is the length of Z^l and $i \in \{0, 1, 2, \ldots, K-1\}$. Finally the whole classifier outputs a predicted label $\hat{y}$ belonging to the input X of the epoch.

2.5 Framework of the Model

Having introduced all the modules, we present the overarching architecture of the model, exemplifying a network that incorporates feature-level fusion. As depicted in Figure 4, the EEG data, following preprocessing, is input into the feature extraction module to derive the EEG feature denoted as V_{eeg}. Similarly, the EMG feature V_{emg} is obtained. The fusion of these two signals yields the fused feature V_{fusion}, subsequently channeled into the feature selection module. Within this module, the processing results in the extraction of the feature V' containing the most informative content for classification. Finally, this feature is employed for classification, resulting in the predicted label $\hat{y}$. This architecture exemplifies the feature-level fusion strategy, showcasing how information from EEG and EMG signals is effectively combined and processed through the various modules of the model to yield a robust and informative classification outcome.

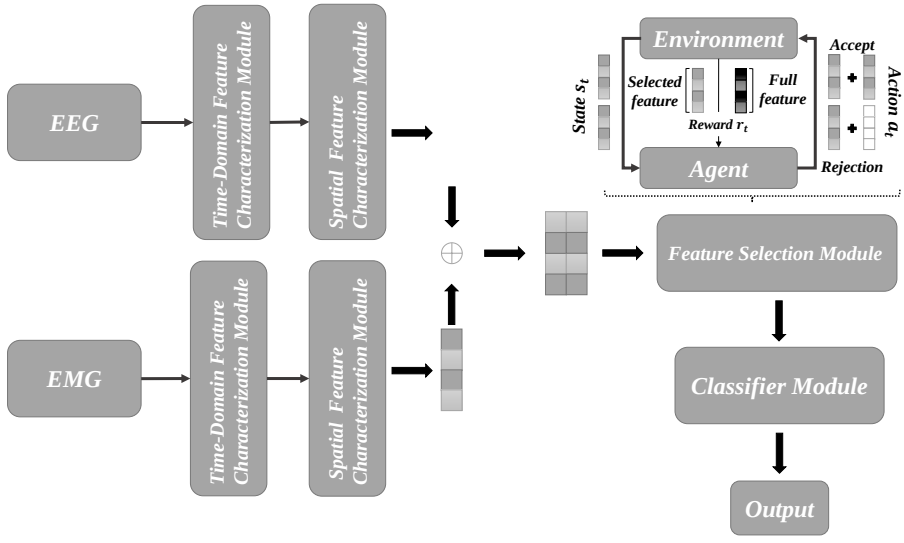

Figure 4. The proposed architectural framework of our model

3 EXPERIMENT AND RESULT

In this section, we will elucidate the dataset utilized for our experiments and expound on the preprocessing steps undertaken. Simultaneously, we will employ this dataset to assess the efficacy of our model, demonstrating its effectiveness through various comparisons.

3.1 Dataset and Preprocessing

We used a publicly available dataset [40] in this experiment that simultaneously captured participants' EEG, EMG, and associated motion information using an inertial measurement unit while they walked on multiple levels of pavement. Ten participants (5 males, 5 females) participated in the dataset, and each participant performed 10 sessions, with each session consisted of a round-trip walk. The experimental paradigm and acquisition setup will be described below, one by one.

The experiment was designed with five stabilized movement patterns (level ground walking (LW), stair descent (SD), stair ascent (SA), ramp descent (RD), and ramp ascent (RA)). Subjects were asked to walk at their preferred speed. Subjects began walking on level ground, walked down the ramp, transitioned to walking on level ground, ascended the stairs, and then rested at the end of the stair landing (in the forward direction). Subjects then turned 180°, walked down the stairs, transitioned to walking on level ground, ascended the ramp, and rested at the end of the ramp landing (reverse direction). Walking in both the forward and reverse directions constituted one complete test trial. Subjects completed an average of 20 trials.

During the experiments, the face and scalp were recorded wirelessly using a 64-channel Ag/AgCl active electrode EEG device (sampling frequency = 1 000 Hz). The TP9, PO9, PO10, and TP10 channels were removed from the cap for electrooculogram (EOG) capture of blinks and eye movements, and the remaining 60 channels were arranged according to the 10–20 international system. Surface EMG signals were recorded at 1 000 Hz using active bipolar electrodes (fixed electrode distance of 20 mm). Surface EMG signals were recorded bilaterally at 6 sites on each leg: the tibialis anterior, gastrocnemius, rectus femoris, vastus lateralis, bicep femoris longus, and the semitendinosus. Seventeen wireless inertial measurement units (IMUs) were also worn by the subjects for whole-body motion capture. IMU data were recorded at 30 Hz and synchronized with EEG time using an external hardware trigger.

For processing and cutting of the dataset, we labeled the time points of different road surfaces based on the inertia and position information recorded by the IMU sensors and converted them to the corresponding points of the EEG and EMG signals for cutting. Based on the sampling frequency of the signals and the relevant a priori knowledge, we chose to take one second of data as a sample, i.e., 1 000 sampling points for each sample. For EEG, we extracted the data from 60 channels and did the re-referencing operation, which is performed with the average of the whole data, i.e., mean-referencing. The purpose is to avoid information loss to some extent. For EMG, the operation is similar to that for EEG, but there is no re-referencing process, and in order to filter the useless clutter information, we performed a band-pass filtering from 1 to 100 Hz to minimize the interference of useless information on the classification.

3.2 Settings and Results

The MUL_RL network with a fusion strategy is used to recognize the ground condition when the subject is moving, the model will be trained for 120 epochs with a batchsize of 64. To optimize the model, we use an $RMSprop$ optimizer with a learning rate of $1e^{-4}$ for the parts outside of reinforcement learning, and for the actor-commentary boundaries network of the reinforcement learning module, we use a learning rationale of $1e^{-2}$ for the $RMSprop$ optimizer for optimization. The training loss for each round is computed uniformly using the previously mentioned cross-entropy loss function. In the evaluation phase, the classification accuracy is used as a metric to assess the performance of the model.

Method	Test Subject										Mean
	Sub1	Sub2	Sub3	Sub4	Sub5	Sub6	Sub7	Sub8	Sub9	Sub10	
CSP + SVM(EEG)	46.84	43.27	49.62	37.94	42.41	39.02	44.59	36.65	39.54	31.07	41.095
CNN(EMG)	46.55	44.85	46.15	43.24	49.42	39.02	44.59	40.31	40.12	49.72	44.397
Data-level + RL	49.43	48.55	45.76	47.06	43.58	42.77	41.31	42.41	32.35	35.03	42.825
Feature-level + RL	**55.17**	**58.05**	**53.85**	**60.88**	**49.42**	46.24	**49.18**	**48.17**	38.89	**53.67**	**51.352**
Decision-level + RL	51.12	55.41	51.15	52.94	49.03	**47.98**	44.26	47.64	**41.83**	46.33	48.769

Table 1. The accuracy of proposed method and comparison method

We evaluated the accuracy of our proposed model in discerning various ground conditions through experiments conducted on all 10 subjects. The results were compared with a baseline model, employing a CSP + SVM architecture for EEG, and a customized CNN model for EMG, respectively. The experimental outcomes, detailed in Table 1, demonstrate the superior performance of our model across all subjects, with an overall higher average accuracy compared to the baseline model. Specifically, among the different fusion strategies, data-level fusion yielded suboptimal results. Only subjects 1, 2, 4, 6, and 8 exhibited improvements over the baseline models, while the average accuracy surpassed the CSP + SVM model but not the common CNN model for myoelectric categorization. In contrast, feature-level fusion consistently outperformed other models on the majority of subjects, excluding subjects 6 and 9. It achieved the best results in terms of accuracy mean, surpassing both data-level and decision-level fusion models. While decision-level fusion exhibited notable efficacy, particularly surpassing feature-level fusion in subjects 6 and 9, it emerged as the most effective model in terms of average accuracy after excluding the feature-level fusion method. In summary, our proposed model, incorporating feature fusion coupled with enhanced feature selection, demonstrates promising results in effectively detecting ground conditions during motion, as evidenced by the experimental outcomes.

To further substantiate the effectiveness of the proposed method, we conducted ablation experiments. Subsequently, we removed the reinforcement feature selection module from the model to assess its impact on classification. The experiments covered various fusion strategies, and the conclusive results are presented in Table 2. Evidently, the classification accuracy of the network employing the reinforced feature

selection module surpassed that without it, across data, feature, and decision-level fusion methods. This improvement held true even when compared to a model utilizing all three feature fusion methods. This underscores the capability of our enhanced feature selection module to identify features conducive to classification while discarding those with minimal or negative impact on enhancing the model's classification effectiveness. Simultaneously, depicted in Figure 5, we showcase the performance of subject 3 in the initial round of ablation experiments using a confusion matrix. The left side represents results from a model employing only feature-level fusion, while the right side incorporates a feature selection module alongside feature-level fusion. Notably, post-feature selection, the model's overall classification accuracy exhibited improvement. Upon detailed categorization, the model demonstrated an impressive nearly 200 % enhancement in the SD category (stair descent). However, there was a simultaneous increase in the model's error rate for misclassifying other categories as SD. Examining other categories, the accuracy for recognizing LW and SA remained relatively stable, while there was a decline in the accuracy for RD and RA categories. This decline is presumed to stem from the model incorrectly identifying less intense slope movements as relatively forceful stepping movements, indicating an area for future model refinement.

Method	Test Subject										Mean
	Sub1	Sub2	Sub3	Sub4	Sub5	Sub6	Sub7	Sub8	Sub9	Sub10	
Data-level	46.84	45.38	43.85	46.76	41.25	40.75	39.34	34.29	31.7	33.9	40.406
Data-level + RL	**49.43**	**48.55**	**45.76**	**47.06**	**43.58**	**42.77**	**41.31**	**42.41**	**32.35**	**35.03**	**42.825**
Feature-level	51.44	55.41	47.69	57.94	49.02	44.22	48.85	41.1	35.62	50.28	48.157
Feature-level + RL	**55.17**	**58.05**	**53.85**	**60.88**	**49.42**	**46.24**	**49.18**	**48.17**	**38.89**	**53.67**	**51.352**
Decision-level	50.57	48.55	43.85	51.18	43.97	41.91	43.28	44.24	39.87	40.96	44.838
Decision-level + RL	**51.12**	**55.41**	**51.15**	**52.94**	**49.03**	**47.98**	**44.26**	**47.64**	**41.83**	**46.33**	**48.769**

Table 2. The accuracy of ablation experiment for feature selection module

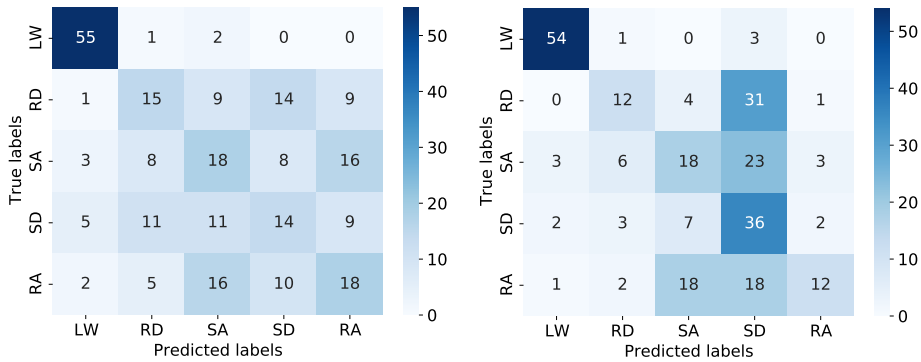

a) Feature-level b) Feature-level + RL

Figure 5. The confusion matrix of subject 3

Method	Test Subject										Mean
	Sub1	Sub2	Sub3	Sub4	Sub5	Sub6	Sub7	Sub8	Sub9	Sub10	
Only EEG	43.97	50.4	40	45.88	36.96	40.75	40.66	36.65	33.99	30.5	39.976
Only EMG	42.53	48.28	46.54	38.53	47.86	39.88	44.92	**46.54**	39.8	**60.84**	45.572
Data-level	46.84	45.38	43.85	46.76	41.25	40.75	39.34	34.29	31.7	33.9	40.406
Feature-level	**51.44**	**55.41**	**47.69**	**57.94**	**49.02**	**44.22**	**48.85**	41.1	35.62	50.28	**48.157**
Decision-level	50.57	48.55	43.85	51.18	43.97	41.91	43.28	44.24	**39.87**	40.96	44.838

Table 3. The accuracy of ablation experiment for fusion theory

For the summarized fusion theory, we opted to utilize EEG and EMG signals without fusion as a baseline to validate the effectiveness of our fusion approach. Table 3 reveals that, while the model employing a single EMG as input (with the exclusion of the reinforcing feature selection module) yielded the best results on subjects 8 and 10, the fusion method outperformed on other subjects, surpassing the baseline in terms of average classification accuracy. Among the three fusion

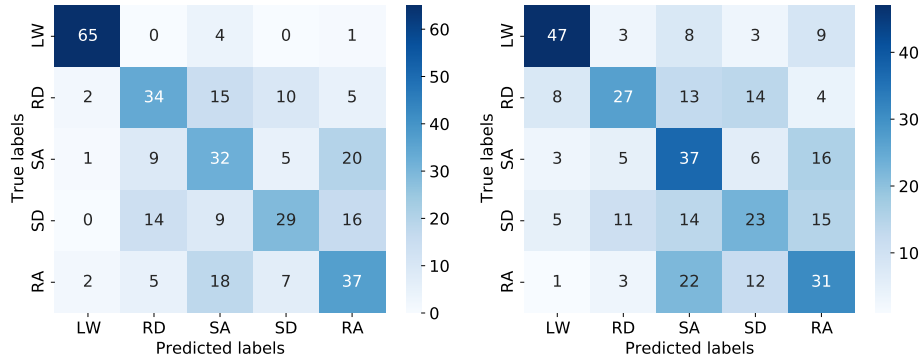

a) Feature-level b) Only EEG

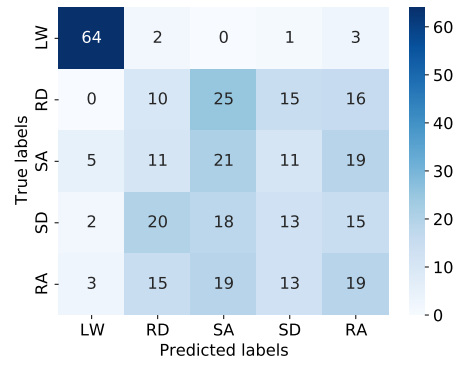

c) Only EMG

Figure 6. The confusion matrix of subject 4

methods, the data-level feature fusion method exhibited suboptimal performance, outperforming the baseline only on subjects 1, 4, and 6. This suggests that data-level fusion, by simply overlaying EEG and EMG data, without considering their deeper features relevant to classification, resulted in a classification effect inferior to single-signal classification. The feature-level fusion method emerged as the most effective, consistently outperforming the other methods. Its accuracy was lower than other methods only on subjects 8, 9, and 10, while it surpassed them in the remaining subjects. The average classification accuracy of the feature-level fusion method also outstripped the other methods. In contrast, the decision-level fusion method showed merit, achieving the highest classification accuracy in subject 9, but its performance varied across other subjects. This variability may be attributed to the limitations of decision-level fusion, which combines classification results from different models akin to ensemble learning but fails to discern invalid information before it interferes with classification. In conclusion, the feature-level fusion method excelled due to its comprehensive integration of extracted features. Despite the potential integration of more invalid information into the feature vector during fusion, the feature information addressing the current ground situation was more complete. Consequently, this method reduced the interference of invalid information, making a substantial contribution to the improvement of classification results.

To delve into the specific performance of the fusion theory, we intricately depicted the experiment's outcomes for subject 4 through a confusion matrix, as illustrated in Figure 6. The top level of the matrix corresponds to the feature-level fusion model, with the lower left section representing the model employing only EEG for classification and the lower right section representing the model using only EMG for classification. Upon inspection, the fusion model showcased superior accuracy compared to the single-signal models in the LW, RD, SD, and RA categories. However, it exhibited a slight decrease in accuracy in the SA category compared to the EEG model, although it remained higher than the EMG model. A holistic view of the EEG model revealed relatively dispersed categorization across individual categories, with notable emphasis on distinguishing RA from SA. The model tended to misclassify RA as SA in the majority of other misclassifications, likely due to both involving upward movements and the topographic information in the signals not being distinctly evident. In contrast, the EMG model displayed the highest differentiation for LW, while internal differentiation among the other four categories was less apparent. The misjudgment rate for RD even surpassed the accuracy rate, possibly because the EMG signal, indicative of sloped motion, differs significantly from that on flat ground. The EMG alone may inadequately capture slope information, leading to incomplete judgments. The fusion model, by amalgamating the strengths of both signals, surpassed the drawbacks. Despite incorporating some shortcomings, the multi-signal feature fusion model outperformed the single-signal model across multiple indicators.

In conjunction with the ablation experiments, we conducted visualizations of intermediate results to elucidate the operational mechanism of the feature selection module and highlight its effectiveness. We selected features extracted by the

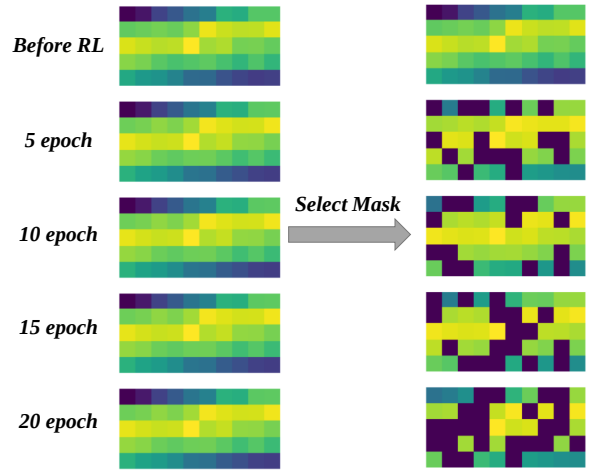

Figure 7. Results of the intermediate feature visualization, left is the feature before feature selection, right is the feature after feature selection

feature selection module at various stages. To facilitate illustration, we mapped these features and presented them in an observable format, as depicted in Figure 7. The rectangles in the figure represent the mapped features. The left column displays the unselected features, the right column showcases features processed by the feature selection module, and the black portion signifies abandoned feature components. Moving from top to bottom in the figure corresponds to different training stages – pre-feature processing module input and states after 5 epochs, 10 epochs, 15 epochs, and 20 epochs of training in the feature processing module. For visualization purposes, LW category data from subject 5 was chosen. A vertical analysis of the left column indicates minimal change in the entire feature matrix. Presumably, this is because the feature extraction module underwent extensive training in prior epochs, fitting the model to the data, resulting in minimal alterations during the feature selection stage. However, upon introducing the selection mask, the associated feature matrix underwent changes, as seen in the right column. At the initial training stages, the selection mask was in the trial phase, and only a few features were discarded. By the 15^{th} epoch of training, more features were discarded, though prominent features, such as those on the rightmost side of the second row and the middle of the third row, were still retained. Similarly, at the 20^{th} epoch, most features on the left side of the matrix were discarded, but significant features persisted. Throughout, the algorithm retained the most favourable features for classification from start to finish.

It is worth noting that during feature selection, in addition to discarding features with minimal contributions, some features with general contributions were also excluded – a minor drawback of the algorithm. Naturally, due to the trial-and-error

nature of reinforcement learning, there are instances where most features are discarded, as illustrated in Figure 8. This data pertains to the RA category for subject 5 during the 15^{th} epoch of training. Notably, a few more apparent features were discarded, leaving only features with average contributions. Presumably, this contributes to the limited improvement in classification accuracy. Addressing how to minimize such occurrences is a consideration for future work, given the algorithm's trial-and-error nature.

Figure 8. Schematic of a negative case of feature selection

4 CONCLUSIONS AND FUTURE WORK

In this paper, we present a classification model that employs a multimodal data fusion strategy and reinforcement learning. The approach integrates reinforcement learning for feature selection and a feature fusion method to enhance the model's classification performance on multimodal data. We conducted experiments using a publicly available web dataset, demonstrating that the model achieved an average classification accuracy of 51.352 % for five classifications. This outperformed other fusion methods and the baseline model (41.095 %), validating the effectiveness of our proposed model. In the related ablation experiments, the feature fusion method exhibited higher classification accuracy than single signal classification. Additionally, the model with the feature selection module surpassed the ordinary model, further supporting the efficacy of our proposed method.

In summary, our contributions can be summarized as follows:

1. We introduce the *MUL_RL* model for detecting and classifying motion intentions in motion execution scenarios. This model uniquely combines a feature fusion strategy with a reinforcement learning-based feature selection approach. The feature fusion strategy extracts feature information from multimodal physiological signals, while the reinforcement learning-based feature selection approach improves classification performance by selecting effective features.
2. A motion intention detection model is designed for motion execution signals instead of motion imagery signals, and the model is validated on relevant datasets to demonstrate the effectiveness of the model. Effective model support is provided for motor rehabilitation training using exoskeletons, and a personalized solution is also provided for motor function rehabilitation.

For the second point, the model is integrated into an assisted movement rehabilitation exoskeleton, collecting EEG and EMG signals from patients through an acquisition device. The model decodes these signals to determine the patient's current

ground environment and provides assistive forces, aiding in neural circuitry rebuilding and motor rehabilitation.

The discussion on multiple feature fusion methods in ablation experiments sheds light on the distinct advantages and disadvantages of single feature fusion methods. However, it underscores the pressing need for experimentation to evaluate the effectiveness of combining multiple fusion methods. Moreover, our feature selection algorithm still has room for improvement, as it may inadvertently discard valid features while eliminating those that contribute minimally to classification. Notably, our validation efforts thus far have been confined to independent subjects, lacking an exploration of the model's effectiveness across different subjects. Additionally, our dataset validation has been primarily focused on the classification performance of healthy human signals, neglecting the unique challenges posed by patient signals. Therefore, our work concludes with discussions on future directions:

- Conduct experiments combining multiple fusion methods to further advance the theory of multimodal data fusion.
- Investigate the model's performance across different subjects using techniques like transfer learning to enhance adaptability to various patient conditions.
- We are committed to enhancing the feature selection algorithm to achieve more refined feature selection and to mitigate the inadvertent discard of effective features.
- Conduct experiments on patient data to compare the model's effects on patients and healthy individuals. Adjust the model architecture to better suit patient needs.

These future efforts aim to enhance the robustness and applicability of the proposed model in diverse scenarios, ultimately contributing to the field of motion intention detection and rehabilitation.

Funding Statement

This work was supported by the Research Project of China Disabled Persons' Federation – on assistive technology, Shanghai Shenkang Hospital Development Center's Second Round of "Three-Year Action Plan to Promote Clinical Skills and Clinical Innovation in Municipal Hospitals" Research Physician Innovation Transformation Capability Training Program (No. SHDC2023CRT001), and the Youth Cross Fund General Project (Medical unit), Henan University (No. S23060Y).

REFERENCES

[1] Wolpaw, J. R.—Birbaumer, N.—McFarland, D. J.—Pfurtscheller, G.—Vaughan, T. M.: Brain–Computer Interfaces for Communication and Control. Clinical Neurophysiology, Vol. 113, 2002, No. 6, pp. 767–791, doi: 10.1016/S1388-2457(02)00057-3.

[2] Yin, Y.—Zheng, X.—Hu, B.—Zhang, Y.—Cui, X.: EEG Emotion Recognition Using Fusion Model of Graph Convolutional Neural Networks and LSTM. Applied Soft Computing, Vol. 100, 2021, Art. No. 106954, doi: 10.1016/j.asoc.2020.106954.

[3] Li, Y.—Xu, Z.—Zhang, Y.—Cao, Z.—Chen, H.: Automatic Sleep Stage Classification Based on a Two-Channel Electrooculogram and One-Channel Electromyogram. Physiological Measurement, Vol. 43, 2022, No. 7, Art. No. 07NT02, doi: 10.1088/1361-6579/ac6bdb.

[4] Liu, W.: Application of EEG in Wearable Brain-Computer Interfaces. International Conference on Intelligent Traffic Systems and Smart City (ITSSC 2021), Proceedings of the SPIE, Vol. 12165, 2022, pp. 464–470, doi: 10.1117/12.2627748.

[5] Shah, S. Y.—Larijani, H.—Gibson, R. M.—Liarokapis, D.: Random Neural Network Based Epileptic Seizure Episode Detection Exploiting Electroencephalogram Signals. Sensors, Vol. 22, 2022, No. 7, Art. No. 2466, doi: 10.3390/s22072466.

[6] Tung, Y. C.—Lai, C. H.—Liao, C. D.—Huang, S. W.—Liou, T. H.—Chen, H. C.: Repetitive Transcranial Magnetic Stimulation of Lower Limb Motor Function in Patients with Stroke: A Systematic Review and Meta-Analysis of Randomized Controlled Trials. Clinical Rehabilitation, Vol. 33, 2019, No. 7, pp. 1102–1112, doi: 10.1177/0269215519835889.

[7] Carvalho, R.—Dias, N.—Cerqueira, J. J.: Brain-Machine Interface of Upper Limb Recovery in Stroke Patients Rehabilitation: A Systematic Review. Physiotherapy Research International, Vol. 24, 2019, No. 2, Art. No. e1764, doi: 10.1002/pri.1764.

[8] Chung, E. J.—Kim, J. H.—Park, D. S.—Lee, B. H.: Effects of Brain-Computer Interface-Based Functional Electrical Stimulation on Brain Activation in Stroke Patients: A Pilot Randomized Controlled Trial. Journal of Physical Therapy Science, Vol. 27, 2015, No. 3, pp. 559–562, doi: 10.1589/jpts.27.559.

[9] Müller-Putz, G. R.—Breitwieser, C.—Cincotti, F.—Leeb, R.—Schreuder, M.—Leotta, F. et al.: Tools for Brain-Computer Interaction: A General Concept for a Hybrid BCI. Frontiers in Neuroinformatics, Vol. 5, 2011, Art. No. 13415, doi: 10.3389/fninf.2011.00030.

[10] Brambilla, C.—Pirovano, I.—Mira, R. M.—Rizzo, G.—Scano, A.—Mastropietro, A.: Combined Use of EMG and EEG Techniques for Neuromotor Assessment in Rehabilitative Applications: A Systematic Review. Sensors, Vol. 21, 2021, No. 21, Art. No. 7014, doi: 10.3390/s21217014.

[11] Yang, H.—Wan, J.—Jin, Y.—Yu, X.—Fang, Y.: EEG- and EMG-Driven Poststroke Rehabilitation: A Review. IEEE Sensors Journal, Vol. 22, 2022, No. 24, pp. 23649–23660, doi: 10.1109/JSEN.2022.3220930.

[12] Zhang, X.—Li, H.—Lu, Z.—Yin, G.: Homology Characteristics of EEG and EMG for Lower Limb Voluntary Movement Intention. Frontiers in Neurorobotics, Vol. 15, 2021, Art. No. 642607, doi: 10.3389/fnbot.2021.642607.

[13] Ak, A.—Topuz, V.—Midi, I.: Motor Imagery EEG Signal Classification Using Image Processing Technique over GoogLeNet Deep Learning Algorithm for Controlling the Robot Manipulator. Biomedical Signal Processing and Control, Vol. 72, Part A, 2022, Art. No. 103295, doi: 10.1016/j.bspc.2021.103295.

[14] Pawuś, D.—Paszkiel, S.: Application of EEG Signals Integration to Proprietary Classification Algorithms in the Implementation of Mobile Robot Control with the Use of Motor Imagery Supported by EMG Measurements. Applied Sciences, Vol. 12, 2022, No. 11, Art. No. 5762, doi: 10.3390/app12115762.

[15] Abdulkader, S. N.—Atia, A.—Mostafa, M. S. M.: Brain Computer Interfacing: Applications and Challenges. Egyptian Informatics Journal, Vol. 16, 2015, No. 2, pp. 213–230, doi: 10.1016/j.eij.2015.06.002.

[16] Tariq, M.—Trivailo, P. M.—Simic, M.: Classification of Left and Right Knee Extension Motor Imagery Using Common Spatial Pattern for BCI Applications. Procedia Computer Science, Vol. 159, 2019, pp. 2598–2606, doi: 10.1016/j.procs.2019.09.256.

[17] Li, M.—Chen, W.: FFT-Based Deep Feature Learning Method for EEG Classification. Biomedical Signal Processing and Control, Vol. 66, 2021, Art. No. 102492, doi: 10.1016/j.bspc.2021.102492.

[18] Gu, L.—Jiang, J.—Han, H.—Gan, J. Q.—Wang, H.: Recognition of Unilateral Lower Limb Movement Based on EEG Signals with ERP-PCA Analysis. Neuroscience Letters, Vol. 800, 2023, Art. No. 137133, doi: 10.1016/j.neulet.2023.137133.

[19] Zhang, T.—Chen, W.—Li, M.: Classification of Inter-Ictal and Ictal EEGs Using Multi-Basis MODWPT, Dimensionality Reduction Algorithms and LS-SVM: A Comparative Study. Biomedical Signal Processing and Control, Vol. 47, 2019, pp. 240–251, doi: 10.1016/j.bspc.2018.08.038.

[20] Zhang, D.—Yao, L.—Chen, K.—Monaghan, J.: A Convolutional Recurrent Attention Model for Subject-Independent EEG Signal Analysis. IEEE Signal Processing Letters, Vol. 26, 2019, No. 5, pp. 715–719, doi: 10.1109/LSP.2019.2906824.

[21] Michielli, N.—Acharya, U. R.—Molinari, F.: Cascaded LSTM Recurrent Neural Network for Automated Sleep Stage Classification Using Single-Channel EEG Signals. Computers in Biology and Medicine, Vol. 106, 2019, pp. 71–81, doi: 10.1016/j.compbiomed.2019.01.013.

[22] Lawhern, V. J.—Solon, A. J.—Waytowich, N. R.—Gordon, S. M.—Hung, C. P.—Lance, B. J.: EEGNet: A Compact Convolutional Neural Network for EEG-Based Brain–Computer Interfaces. Journal of Neural Engineering, Vol. 15, 2018, No. 5, Art. No. 056013, doi: 10.1088/1741-2552/aace8c.

[23] Chen, J.—Jiang, D.—Zhang, Y.—Zhang, P.: Emotion Recognition from Spatiotemporal EEG Representations with Hybrid Convolutional Recurrent Neural Networks via Wearable Multi-Channel Headset. Computer Communications, Vol. 154, 2020, pp. 58–65, doi: 10.1016/j.comcom.2020.02.051.

[24] Sairamya, N. J.—Subathra, M. S. P.—George, S. T.: Automatic Identification of Schizophrenia Using EEG Signals Based on Discrete Wavelet Transform and RLNDiP Technique with ANN. Expert Systems with Applications, Vol. 192, 2022, Art. No. 116230, doi: 10.1016/j.eswa.2021.116230.

[25] Neeraj, N.—Singhal, V.—Mathew, J.—Behera, R. K.: Detection of Alcoholism Using EEG Signals and a CNN-LSTM-ATTN Network. Computers in Biology and Medicine, Vol. 138, 2021, Art. No. 104940, doi: 10.1016/j.compbiomed.2021.104940.

[26] He, H.—Wu, D.: Transfer Learning for Brain-Computer Interfaces: A Euclidean Space Data Alignment Approach. IEEE Transactions on Biomedical Engineering, Vol. 67, 2019, No. 2, pp. 399–410, doi: 10.1109/TBME.2019.2913914.

[27] Pan, S. J.—Yang, Q.: A Survey on Transfer Learning. IEEE Transactions on Knowledge and Data Engineering, Vol. 22, 2009, No. 10, pp. 1345–1359, doi: 10.1109/TKDE.2009.191.

[28] An, S.—Kim, S.—Chikontwe, P.—Park, S. H.: Few-Shot Relation Learning with Attention for EEG-Based Motor Imagery Classification. 2020 IEEE/RSJ International Conference on Intelligent Robots and Systems (IROS), 2020, pp. 10933–10938, doi: 10.1109/IROS45743.2020.9340933.

[29] Wei, Y.—Li, J.—Ji, H.—Jin, L.—Liu, L.—Bai, Z.—Ye, C.: A Semi-Supervised Progressive Learning Algorithm for Brain–Computer Interface. IEEE Transactions on Neural Systems and Rehabilitation Engineering, Vol. 30, 2022, pp. 2067–2076, doi: 10.1109/TNSRE.2022.3192448.

[30] Ko, W.—Jeon, E.—Yoon, J. S.—Suk, H. I.: Semi-Supervised Generative and Discriminative Adversarial Learning for Motor Imagery-Based Brain–Computer Interface. Scientific Reports, Vol. 12, 2022, No. 1, Art. No. 4587, doi: 10.1038/s41598-022-08490-9.

[31] Arulkumaran, K.—Deisenroth, M. P.—Brundage, M.—Bharath, A. A.: Deep Reinforcement Learning: A Brief Survey. IEEE Signal Processing Magazine, Vol. 34, 2017, No. 6, pp. 26–38, doi: 10.1109/MSP.2017.2743240.

[32] François-Lavet, V.—Henderson, P.—Islam, R.—Bellemare, M. G.—Pineau, J.: An Introduction to Deep Reinforcement Learning. Foundations and Trends® in Machine Learning, Vol. 11, 2018, No. 3-4, pp. 219–354, doi: 10.1561/2200000071.

[33] Wang, S.—Tang, H.—Wang, B.—Mo, J.: A Novel Approach to Detecting Muscle Fatigue Based on sEMG by Using Neural Architecture Search Framework. IEEE Transactions on Neural Networks and Learning Systems, Vol. 34, 2023, No. 8, pp. 4932–4943, doi: 10.1109/TNNLS.2021.3124330.

[34] Zhang, Q.—Nalam, V.—Tu, X.—Li, M.—Si, J.—Lewek, M. D.—Huang, H. H.: Imposing Healthy Hip Motion Pattern and Range by Exoskeleton Control for Individualized Assistance. IEEE Robotics and Automation Letters, Vol. 7, 2022, No. 4, pp. 11126–11133, doi: 10.1109/LRA.2022.3196105.

[35] Ming, Y.—Wu, D.—Wang, Y. K.—Shi, Y.—Lin, C. T.: EEG-Based Drowsiness Estimation for Driving Safety Using Deep Q-Learning. IEEE Transactions on Emerging Topics in Computational Intelligence, Vol. 5, 2021, No. 4, pp. 583–594, doi: 10.1109/TETCI.2020.2997031.

[36] Ko, W.—Jeon, E.—Suk, H. I.: A Novel RL-Assisted Deep Learning Framework for Task-Informative Signals Selection and Classification for Spontaneous BCIs. IEEE Transactions on Industrial Informatics, Vol. 18, 2022, No. 3, pp. 1873–1882, doi: 10.1109/TII.2020.3044310.

[37] Noori, F. M.—Riegler, M.—Uddin, M. Z.—Torresen, J.: Human Activity Recognition from Multiple Sensors Data Using Multi-Fusion Representations and CNNs. ACM Transactions on Multimedia Computing, Communications, and Appli-

cations (TOMM), Vol. 16, 2020, No. 2, Art. No. 45, doi: 10.1145/3377882.

[38] Kim, H.—Lee, S. M.—Choi, S.: Automatic Sleep Stages Classification Using Multi-Level Fusion. Biomedical Engineering Letters, Vol. 12, 2022, No. 4, pp. 413–420, doi: 10.1007/s13534-022-00244-w.

[39] Ko, W.—Jeon, E.—Jeong, S.—Suk, H. I.: Multi-Scale Neural Network for EEG Representation Learning in BCI. IEEE Computational Intelligence Magazine, Vol. 16, 2021, No. 2, pp. 31–45, doi: 10.1109/MCI.2021.3061875.

[40] Brantley, J. A.—Luu, T. P.—Nakagome, S.—Zhu, F.—Contreras-Vidal, J. L.: Full Body Mobile Brain-Body Imaging Data During Unconstrained Locomotion on Stairs, Ramps, and Level Ground. Scientific Data, Vol. 5, 2018, Art. No. 180133, doi: 10.1038/sdata.2018.133.

Liujie Cheng received his B.Sc. degree in information security from the Tongji University in 2021. Now, he is a graduate student in the Department of Computer Science and Technology, Tongji University. His research interests include machine learning and brain-computer interface.

Hongfei Ji is Associate Professor with the Department of Computer Science and Technology, Tongji University, Shanghai, China. He received his Ph.D. degree in software engineering from the Tongji University, Shanghai, China, in 2015. His research interests include machine learning, pattern recognition, brain computer interface, and cognitive neuroscience.

Jie Li is Associate Professor at the Department of Computer Science and Technology, Tongji University, Shanghai, China. She received her Ph.D. degree in computer science from Shanghai Jiao Tong University, Shanghai, China, in 2010. Her research interests include machine learning, brain computer interface, brain like computation, and cognitive neuroscience.

Jian Yu is Engineer at the Department of Lab Center, School of Electronic and Information Engineering, Tongji University, Shanghai, China. He received his Ph.D. degree in circuits and systems from the South China University of Technology, Guangzhou, in 2010. His research interests include Internet of Things, machine learning, pattern recognition, and embedded systems.

Zilong Pang is Lecturer with the School of Software, Henan University, China. He received his Master's degree in applied mathematics in computer science and Ph.D. at the College of Electronic and Information Engineering, Tongji University, China. His research directions mainly include brain computer interface, artificial intelligence in medical imaging, machine vision.